Slow Photo-Cross-Linking Kinetics of Benzophenone-Labeled Voltage Sensors of Ion Channels†

Shinghua Ding and Richard Horn*

Department of Physiology, Institute of Hyperexcitability, Jefferson Medical College, 1020 Locust Street, Philadelphia, Pennsylvania 19107

Received April 6, 2001; Revised Manuscript Received June 13, 2001

ABSTRACT: Voltage-gated ion channels have voltage sensors that move in response to changes in membrane potential. This movement regulates the gates that control access of ions to the permeation pathway. To study the coupling between voltage sensors and gates, we immobilize the voltage sensors, using a bifunctional photo-cross-linking reagent that can be attached to an introduced cysteine, and observe the consequences for gate movement [Horn, R., Ding, S., and Gruber, H. J. (2000) *J. Gen. Physiol. 116*, 461−475]. UV irradiation of the benzophenone adduct attached to the cysteine residue immobilizes the voltage sensors, S4 segments, of both Na^+ and *Shaker* K^+ channels. Here we examine the kinetics of S4 immobilization after a brief UV flash. Immobilization has an exponential time course with time constants of >200 ms for *Shaker* and 17 ms for Na^+ channels, whereas the triplet excited state lifetime of the benzophenone adduct is <1 ms. This result suggests that H-atom abstraction by benzophenone is rapid and that the rate-limiting step in immobilization is the recombination of alkyl and ketyl free radicals generated by H-abstraction. H-Abstraction is also 2.7-fold more efficient at a hyperpolarized voltage than at a depolarized membrane potential in *Shaker* S4 segments. S4 immobilization after a UV flash can be prevented by depolarization of *Shaker* channels, suggesting that movement in the activation pathway is capable of separating the ketyl and alkyl free radicals. Exploiting the unique charge movement and gating properties of the L382V mutant of *Shaker*, we show that free radical separation follows S4 movement itself and is relatively independent of the movement of activation gates.

Ion channels are transmembrane proteins with a permeation pathway (i.e., pore) through which ions can diffuse down their electrochemical gradients. Voltage-dependent ion channels respond to changes in membrane potential by opening or closing the pore. The members of this superfamily of ion channels have a tetrameric structure, consisting of either four homologous or identical subunits, as in K^+ channels, or four homologous domains of a single polypeptide, as in Na^+ and Ca^{2+} channels (*1*). Each subunit or domain has cytoplasmic N- and C-termini and six transmembrane segments, S1−S6.

Voltage-dependent channels have at least two types of moving parts, charged voltage sensors that move in response to changes in membrane potential and gates that control access of permeant ions to the pore (*2*−*5*). The main voltage sensors are positively charged S4 segments, and gates are located at both the extracellular and cytoplasmic entrances to the permeation pathway. The initial step after a depolarization is the displacement (an outward movement) of positively charged amino acid side chains in the S4 segments (*6*); this charge movement generates an outward gating current. Following the S4 movement the activation gate opens, allowing ion conduction through the pore. In some channels, maintained depolarization may cause the closing of either fast or slow inactivation gates. Although we have excellent candidates for the regions of the protein that serve as voltage sensors, gates, and the pore (*3*−*5*, *7*), we can only speculate about how the movement of S4 segments triggers the channel gates to open and close.

To tackle this problem of the coupling between voltage sensors and gates, we recently began to explore the possibility of systematically immobilizing the moving parts, using a bifunctional photoactivatable cross-linker, benzophenone-4-carboxamidocysteine methanethiosulfonate (BPMTS),[1] that can be tethered to cysteines introduced into the channel protein by mutagenesis (*8*). Our results indicated that we could use UV irradiation to immobilize individual S4 segments and an inactivation gate of Na^+ channels.

While studying the immobilization of the S4 segment of *Shaker* K^+ channels, we noticed that cross-linking kinetics after a UV flash delivered by a xenon flashlamp were >2 orders of magnitude slower than the triplet state lifetime of benzophenone (*9*, *10*), the photoactive component of BPMTS. Here we exploit these slow kinetics to explore voltage-dependent movements in the vicinity of the S4 segment.

† Supported by National Institutes of Health Grant AR41691.

* To whom correspondence should be addressed: Department of Physiology, Institute of Hyperexcitability, Thomas Jefferson University, 1020 Locust St., Philadelphia, PA 19107. E-mail: Richard.Horn@TJU.edu. Telephone: (215) 503-6725. Fax: (215) 503-2073.

[1] Abbreviations: BPMTS, benzophenone-4-carboxamidocysteine methanethiosulfonate; BP, benzophenone; H-abstraction, hydrogen-atom abstraction. Throughout the paper, we use the single-letter code to designate the amino acids and point mutations

10.1021/bi010709y CCC: $20.00
Published on Web 08/08/2001

EXPERIMENTAL PROCEDURES

Mutants and Transfection. We used a *Shaker*-IR K^+ channel cDNA clone in which N-type inactivation is removed by deletion of a portion of the cytoplasmic NH_2 terminus and C-type inactivation is partially inhibited by the T449V point mutation (*11*) in the pGW1-CMV vector (British Biotechnology, Oxford, U.K.). Four different mutants based on this background were used: A359C and its nonconducting version with the W434F pore mutation (A359C/W434F) and the double mutant A359C/L382V and its nonconducting version (A359C/L382V/W434F). A359 is located near the extracellular end of *Shaker*'s S4 segment. In the human skeletal muscle Na^+ channel ($hNa_V1.4$), we used a cysteine substitution for the outermost arginine of the S4 segment of the second homologous domain, D2:R1C (R669C); this clone was inserted into the pRC-CMV vector. Mutagenesis was carried out with QuickChange site-directed mutagenesis kits from Stratagene (La Jolla, CA). All of the cDNA clones were sequenced to verify the mutations.

The mutant DNA was transfected into tsA201 cells, a transformed mammalian cell line, using a standard calcium phosphate method. After 6−12 h, the transfected cells were passed onto 25 mm round, glass coverslips in Petri dishes. The glass coverslips were used as the bottom of a chamber mounted on the stage of an inverted compound microscope (TE-300 Eclipse from Nikon, Tokyo, Japan) for electrophysiological experiments.

Electrophysiology and Data Acquisition. Standard whole-cell recording methods were used to record gating and ionic currents with an AXOPATCH 200B amplifier (Axon Instruments, Foster City, CA) (*8*). For the A359C, A359C/W434F, A359C/L382V/W434F, and D2:R1C mutants, the patch pipet contained 105 mM CsF, 35 mM NaCl, 10 mM EGTA, and 10 mM Hepes (pH 7.4). The bath contained 150 mM NaCl, 2 mM KCl, 1.5 mM $CaCl_2$, 1 mM $MgCl_2$, and 10 mM Hepes (pH 7.4). For the A359C/L382V mutant channel ionic currents, the pipet contained 52.5 mM CsF, 52.5 mM KF, 35 mM NaCl, 10 mM EGTA, and 10 mM Hepes (pH 7.4). The bath solution remained the same as for the other mutants.

All of the experiments were carried out at room temperature. Liquid junction potentials were corrected. The electrode resistance was in the range of 1−2 MΩ. Voltage errors due to series resistance were <3 mV after compensation. Data were low-pass filtered at 5−10 kHz and acquired with a DigiData 1200B digitizer using Clampex 8.0 (Axon Instruments). Gating and ionic currents were obtained using a P/-8 correction protocol for capacitance and leakage subtraction from holding potentials more negative than −110 mV.

Chemicals and Labeling. Benzophenone-4-carboxamidocysteine methanethiosulfonate (BPMTS) was purchased from Toronto Research Chemicals (North York, ON).

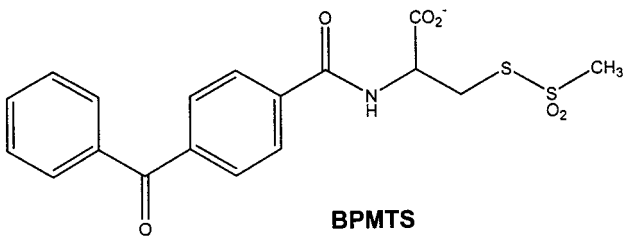

BPMTS

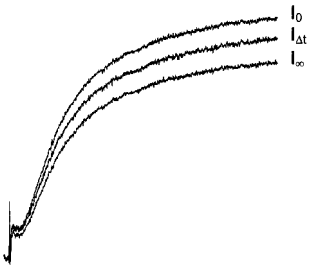

FIGURE 1: Current traces for analyzing S4 segment immobilization. Currents generated by depolarizations to 20 mV. I_0 is the current measured before UV irradiation, $I_{\Delta t}$ the current measured at Δt (milliseconds) after a UV flash ($\Delta t = 200$ ms in this experiment), and I_∞ the current measured after the photo-cross-linking reaction to the flash is complete (in most of our cases, 3 s after irradiation).

Extracellular labeling of cysteines was carried out by treating a coverslip of attached cells with 1 mM BPMTS for 10 min. We added 50 mM KCl to the bath solution during labeling to depolarize the cells and expose all the S4 segments to the reagent. All other chemicals were purchased from Sigma (St. Louis, MO).

Photo-Cross-Linking. Benzophenone was activated by UV light presented to a voltage-clamped cell through a 40× (1.3 N.A.) oil immersion objective (S-Fluor, Nikon). The UV light source triggered by the data acquisition system was a xenon flash lamp (Rapp Opto Electronic). We used a DET210 high-speed photodiode (ThorLab Inc., Newton, NJ) to measure the time course of the UV flash. Light was band-pass filtered between 340 and 390 nm to avoid photodamage.

Data Analysis. Data were analyzed by a combination of CLAMPFIT 8.0 (Axon Instruments) and ORIGIN 6.0 (MicroCal, Northampton, MA). Throughout the paper, the vertical bars in graphs represent the standard error of the mean.

Because of the tetrameric symmetry of *Shaker* potassium channels, the reduction of ionic current due to a flash of UV light is not an exact representation of the immobilization of individual S4 segments (*8*). Figure 1 shows an example of the ionic current before a flash (labeled I_0), at time Δt after a flash (labeled $I_{\Delta t}$), and 3 s after the flash (labeled I_∞), when the immobilization is complete.

Let $p_I(\infty)$ ($=I_\infty/I_0$) be the total reduction of ionic current caused by a UV flash, and let $p_I(\Delta t)$ ($=I_{\Delta t}/I_0$) be the reduction of ionic current at time Δt after a flash. The fractional reduction of ionic current at time Δt after a flash is

$$\frac{\Delta I}{I} = \frac{1 - p_I(\Delta t)}{1 - p_I(\infty)}$$

Because of tetrameric symmetry, the fractional immobilization of S4 segments is given by

$$\frac{\Delta Q}{Q} = \frac{1 - [p_I(\Delta t)]^{1/4}}{1 - [p_I(\infty)]^{1/4}}$$

where Q represents the S4 charge movement and $\Delta Q/Q$ is the fractional charge immobilization at time Δt after a flash. In general, $\Delta Q/Q$ is less than $\Delta I/I$.

RESULTS

Voltage-Dependent S4 Immobilization. Depolarization of voltage-dependent ion channels causes an outward displace-

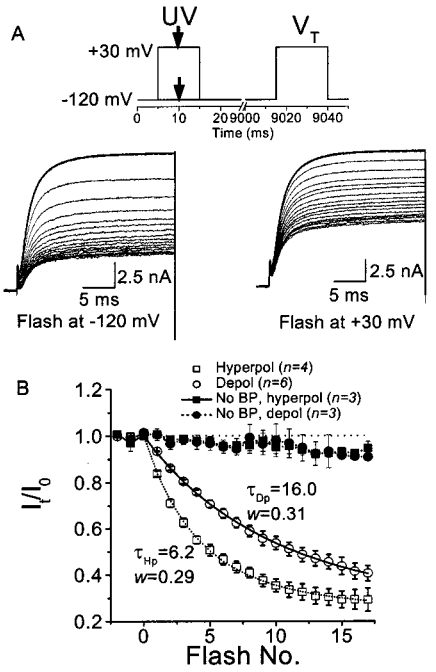

FIGURE 2: Effect of voltage of UV irradiation on the ionic current reductions of *Shaker*-IR A359C-BP. (A) The voltage protocol is shown at the top. The arrow indicates the UV irradiation at either 120 or 30 mV. Currents were measured with a test voltage (V_T) at 30 mV during repeated UV irradiation (11 s between flashes) at hyperpolarized (lower left) and depolarized (lower right) voltages. The largest current traces in each case were measured before UV irradiation. (B) The reductions of current at depolarized (○) and hyperpolarized (□) voltages as a function of the number of flashes. The smooth curves are the fits by a single-exponential function raised to a fourth power $\{I_t/I_0 = [(1 - \omega) + \omega e^{-t/\tau}]^4\}$ (*8*). The time constant τ is the number of flashes. The currents were normalized to the current before UV irradiation. The normalized currents from unlabeled channels were measured after irradiation at hyperpolarized (●) or depolarized (■) voltages.

ment of positively charged S4 segments across the membrane electrical field (*12*−*14*). This charge movement can be observed as a transient outward gating current, which is followed by opening of activation gates, producing an ionic current through the open channels. The outward S4 movement is believed to be required for the activation gates to open. Accordingly, immobilization of the S4 segment of *Shaker* potassium channels, by irradiation of BPMTS-labeled residue A359C, reduces both the gating current and ionic current (*8*). We reported previously that the UV irradiation is more effective when applied at a hyperpolarized membrane potential, suggesting that the BP adduct can more easily find an insertion site when the S4 segment is retracted inward (*8*). We examine this phenomenon quantitatively here.

Figure 2 shows that a UV flash immobilizes S4 segments more efficiently at −120 mV than at 30 mV. The stimulation protocol is shown in Figure 2A along with representative current traces in response to a series of UV flashes at either the hyperpolarized (left) or depolarized (right) voltage. The largest control currents (three superimposed traces) were obtained before exposure to UV. These ionic currents were measured at a test voltage of 30 mV. Figure 2B shows that the current reduction for irradiation at the hyperpolarized voltage is faster than at the depolarized voltage. It also shows that unlabeled channels are relatively insensitive to UV irradiation, regardless of the membrane potential. We showed

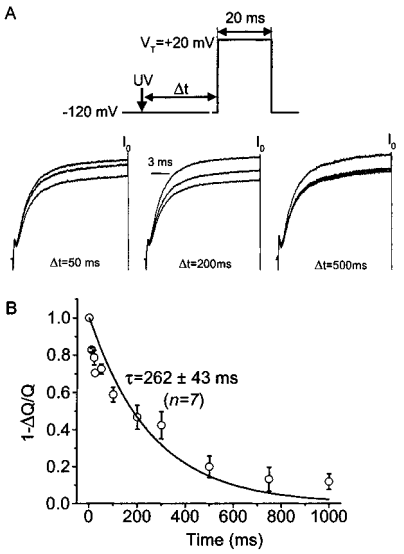

FIGURE 3: Slow kinetics of photo-cross-linking of *Shaker*-IR A359C-BP. (A) The experimental protocol is shown at the top. The cells were irradiated at −120 mV, as denoted with an arrow, and after Δt (milliseconds), a test pulse V_T of 20 ms was applied at 20 mV. Typical currents measured at different values of Δt after irradiation. In each panel, the largest current trace (I_0) is measured before irradiation as a control, the intermediate trace is the current after Δt (milliseconds) of irradiation, and the smallest current is after 3 s, when the photo-cross-linking in response to that flash is finished (also see Experimental Procedures and Figure 1). The currents were scaled to the same initial amplitude in each panel. (B) The time course of $1 - \Delta Q/Q$. The solid line is a fit of a single-exponential function: $1 - \Delta Q/Q = e^{-t/\tau}$ with a time constant τ of 262 ms ($n = 7$).

previously that S4 immobilization is a first-order process (*8*). Because of the tetrameric stoichiometry of the *Shaker* channel, the probability of a channel being functional is the fourth power of S4 functionality. Therefore, we fit the normalized ionic current reduction to a single-exponential function raised to a fourth power (Figure 2B). The time constants from these fits represent those of S4 immobilization, which is 2.7-fold faster when flashed at the hyperpolarized voltage than at a depolarized voltage. This is consistent with the idea that the BP adduct can find its target more readily at the hyperpolarized voltage. The total percentage of immobilized S4 segments after saturating irradiation (∼30%) was similar for each membrane potential.

Slow Kinetics of S4 Segment Immobilization. While carrying out the aforementioned experiments, we observed that the ionic current did not exhibit a complete reduction until hundreds of milliseconds after a UV flash with a duration of ∼580 μs. This is shown in Figure 3. A UV flash at the −120 mV holding potential was followed, after a variable interval (Δt), by a depolarization to 20 mV to measure the ionic current. In each of three panels (Δt values of 50, 200, and 500 ms), three current traces are shown (Figure 3A). The trace labeled I_0 is the ionic current 3 s before the UV flash; the middle trace is the current at time Δt after the flash, and the lowermost trace is the current 3 s later. Subsequent depolarizations showed no further change in current amplitude (not shown). Figure 3B shows the analysis of the data from seven cells, with current reduction after Δt transformed to represent S4 immobilization (see Experimental Procedures). The data were fit to an exponential function with a time constant of 262 ms. We interpret these

Scheme 1

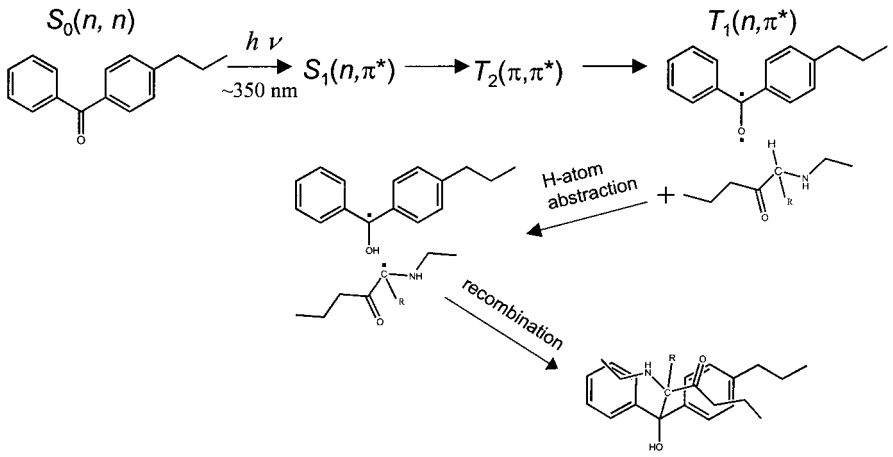

results as an indication of the slow kinetics of cross-linking of individual S4 segments after a UV flash. What is the rate-limiting step in cross-linking kinetics?

Scheme 1 shows the sequence of photochemical reactions for BP-based cross-linking (*9*, *10*). Absorption of a photon at ~350 nm generates a singlet excited state $S_1(n,\pi^*)$ which generates a triplet excited state $T_1(n,\pi^*)$, after passing through $T_2(n,\pi^*)$. Passage from $S_1(n,\pi^*)$ to $T_1(n,\pi^*)$ occurs with a quantum yield close to unity. The triplet biradical $T_1(n,\pi^*)$ will insert into a C−H bond, with a mild preference for the α-carbon of a peptide backbone. The insertion typically takes place in two steps. First, a hydrogen is abstracted (H-abstraction). This is followed by a recombination of the alkyl and ketyl free radicals generated during H-abstraction. At least one of these steps must be slow enough to account for the data depicted in Figure 3.

We consider the individual steps in sequence. The delay in triggering the flash lamp was <10 μs, and we measured the duration of the flash (fwhm) as 580 μs. Both $S_1(n,\pi^*)$ and $T_2(\pi^*,\pi^*)$ are very short-lived intermediates with lifetimes of <100 ps (*10*). The triplet biradical, $T_1(n,\pi^*)$, has a longer lifetime, but it is also <1 ms in the absence of an H-atom donor (*10*). The lifetime is decreased in the presence of an abstractable H-atom according to the Stern−Volmer relationship (*10*).

On the basis of the arguments presented above, the rate-limiting step in cross-linking is likely to be the recombination between ketyl and alkyl free radicals after H-atom abstraction. Note that slow recombination implies that the free radicals persist long enough to be able to react hundreds of milliseconds after they are generated. This raises the possibility that they might be destroyed before recombination can occur, for example, by reaction with nonradical substrates. We will consider these issues in the Discussion.

If recombination is rate-limiting, we can interpret the voltage-dependent rates of cross-linking of Figure 2 as a consequence of more efficient H-atom abstraction at a hyperpolarized voltage. This conclusion follows from the fact that (i) recombination is insignificant during the 5 ms after a flash at the depolarized voltage (Figure 6A) and (ii) the time between flash and test depolarization is long enough (9 s) for recombination at −120 mV to be complete for an individual flash.

The results depicted in Figure 3 indicate that recombination is slow, which may be a consequence of the local environment near the labeled A359C residue in *Shaker*. To further explore this possibility, we examined the cross-linking kinetics of a cysteine mutant in the S4 segment of the $hNa_V1.4$ Na^+ channel under identical conditions (Figure 4). The time constant of photo-cross-linking is ~17 ms for this mutant, which is ~15-fold faster than the kinetics of the *Shaker* mutant, but it is still much slower than either the flash duration or the expected triplet state lifetime of BP. Therefore, recombination is also rate-limiting in this case. The different kinetics of the Na^+ channel mutant D2:R1C and the *Shaker*-IR K^+ channel mutant A359C indicate that cross-linking kinetics depend on the structural differences experienced by the BP moiety tethered to the S4 cysteines of these two mutants.

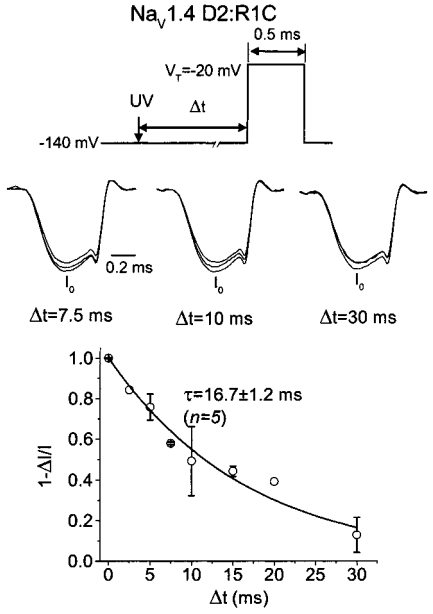

FIGURE 4: Faster kinetics of photo-cross-linking for the S4 segment in domain II of the Na^+ channel (D2:R1C-BP). (A) The experimental protocol is shown at the top. UV radiation was flashed at the −140 mV holding potential as denoted with an arrow, and after Δ*t* (milliseconds), a test pulse of 0.5 ms was applied at −20 mV. (B) Typical inward currents measured at different values of Δ*t* after irradiation. The control currents (largest) are indicated as I_0. (C) Time course of $1 - \Delta I/I$. The data were fit with a single-exponential function as in Figure 3 with a time constant τ of 16.7 ms ($n = 5$).

Voltage Dependence of Recombination. We ask here whether the alkyl and ketyl free radicals generated by H-atom abstraction can be separated physically, thereby preventing

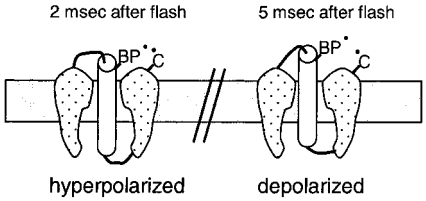

FIGURE 5: Strategy for voltage-dependent effects on recombination rates. A single K^+ channel subunit with a BP-labeled S4 segment is drawn as a tethered cylinder that can be moved by voltage through a gating pore. The left cartoon shows the subunit 2 ms after a UV flash at a hyperpolarized voltage, indicating the unreacted ketyl and alkyl free radicals. The right cartoon shows the same subunit 5 ms after the flash when a depolarization is applied. In response to the depolarization, the S4 segment has translocated outward, carrying its ketyl free radical on the BP.

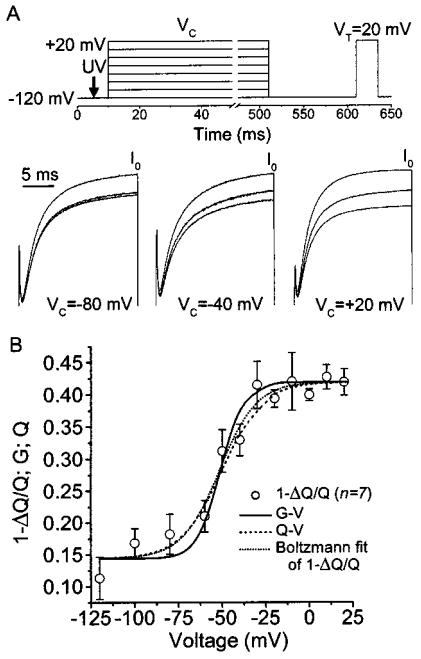

FIGURE 6: Voltage dependence of S4 segment immobilization of the A359C-BP mutant. (A) The voltage protocol is shown at the top. A 500 ms conditioning prepulse (V_C) with 20 mV increments from −120 to 20 mV was followed by a 100 ms hyperpolarized pulse at −120 mV, and then by a 25 ms test voltage (V_T) at 20 mV. UV radiation was delivered at the −120 mV holding potential 5 ms prior to V_C. Typical currents with different values of V_C show different fractional reductions after irradiation. Note that the total reduction for a single flash depends primarily on the number of unreacted BP adducts on the channels, rather than on V_C (see Figure 2). (C) The $(1 - \Delta Q/Q) - V$ relationship ($n = 7$). The solid curve is a fit to a single-Boltzmann function with a $V_{1/2}$ of -51.8 ± 3.1 mV and a q of 2.3 ± 0.7 e_o. $G-V$ and $Q-V$ curves from Figure 7 are scaled and superimposed.

or slowing recombination. This question can be answered experimentally because (i) we can generate the free radicals rapidly by a flash of UV light, (ii) recombination is very slow, especially for the *Shaker* mutant, and (iii) we can produce a rapid conformational change in the ion channel by applying a depolarizing voltage step shortly after the UV flash. This strategy is shown in Figure 5 which depicts a single K^+ channel subunit with a BP-labeled S4 segment, drawn as a tethered cylinder that can be moved by voltage through a gating pore. The left cartoon shows the subunit 2 ms after a flash at a hyperpolarized voltage and indicates that the UV has caused H-atom abstraction, leaving unreacted ketyl and alkyl free radicals. The right cartoon shows what might happen if a depolarization is applied 5 ms after the flash. The S4 segment has translocated outward, carrying its ketyl free radical on the BP. This, or another, voltage-dependent movement of the S4 segment might separate the free radicals, decreasing the rate of recombination.

To test this hypothesis, we carried out the following experiment with the BP-labeled *Shaker*-IR mutant A359C. Five milliseconds after a flash at −120 mV, we depolarized the cell for 500 ms (voltage protocol in Figure 6A). After a 100 ms return to the holding potential, during which some recombination could take place, we measured the current in response to a test pulse at 20 mV. The total extent of recombination due to the UV flash is assessed by another test pulse 3 s later. As in Figures 3 and 4, three test depolarizations were given: before the flash (labeled I_0), after the flash (intermediate), and 3 s later (smallest current) when the cross-linking for that single flash was complete. Our hypothesis is that if a large depolarization can separate the free radicals sufficiently, then no recombination will occur during the 500 ms depolarization, and the fractional recombination measured in the subsequent depolarization will be due only to whatever occurred at −120 mV (a total of 105 ms after the flash, Figure 6A). The expected amount of cross-linking at −120 mV can be determined exactly from the results depicted in Figure 3. Note the fundamental difference between the results of this experiment and those shown in Figure 2, where UV was flashed at either a hyperpolarized or a depolarized voltage. In the experiment whose results are depicted in Figure 6, the flash was always applied at the hyperpolarized voltage, but the voltage at which recombination occurred was changed systematically.

As hypothesized, prolonged depolarization after a flash does inhibit recombination. Figure 6 shows only moderate cross-linking after a 500 ms depolarization to 20 mV. The ∼60% current reduction after the step to 20 mV (Figure 6A, right panel) is larger, however, than the ∼40% reduction predicted for 105 ms at −120 mV (Figure 3B). This shows that the rate of recombination is slowed, but not arrested, by the 500 ms depolarization. Note that if the membrane potential is maintained at −120 mV for 605 ms, the duration between the flash and the test depolarization, the current is reduced by ∼90% (Figure 3). Taken together, these results show that the 500 ms depolarization to 20 mV significantly inhibits recombination. The rate of recombination at 20 mV can be estimated directly, if the depolarization is assumed to decrease the rate rapidly to a fixed value. Using the theoretical curve from Figure 3 and the mean data at 20 mV from Figure 6B, we estimate the recombination time constant at 20 mV (τ_{+20}) from the following relationship

$$e^{-(500/\tau_{+20})} = f_a e^{+(105/\tau_{-120})}$$

where the time constants of recombination at 20 and −120 mV are given in milliseconds and f_a is the measured fraction of available (i.e., not immobilized) S4 segments after 500 ms at 20 mV and after 105 ms at −120 mV. From Figure 6B, $f_a = 0.419$. Solving for τ_{+20}, we find that the recombination rate is 3.9-fold faster at −120 mV than at 20 mV.

Figure 6 also depicts the shape of the voltage dependence of the extent of recombination, as measured by $1 - \Delta Q/Q$ (see Experimental Procedures), which has a monotonic sigmoidal voltage dependence, saturating at extremes of

hyperpolarization and depolarization. We fit the data with a Boltzmann function having a midpoint of -51.8 ± 3.1 mV and a slope equivalent to the movement of 2.3 ± 0.7 elementary charges (e_0) through the membrane electric field (Figure 6B).

Why does membrane potential affect the rate of recombination? If the inhibition of recombination is due to a physical separation of the alkyl and ketyl free radicals generated by the UV flash, then the voltage-dependent recombination rate is a reflection of a voltage-dependent movement in the vicinity of the S4 segment. What conformational change is responsible for this voltage-dependent movement? Two different voltage-dependent conformational changes are likely candidates for causing the separation of the alkyl and ketyl free radicals. The first is S4 movement itself; the second involves the conformational rearrangements associated with movement of either activation or inactivation gates. S4 movement is responsible for most of the gating current (*4*, *15*, *16*). Therefore, the classical $Q-V$ relationship for gating current is an estimate, albeit biased (*16*), of the steady state voltage dependence of S4 movement. For the *Shaker* mutant we use, there is no N-type inactivation, and C-type inactivation is strongly inhibited (*17*). Therefore, voltage-dependent movement of gates in these channels is mainly restricted to the process of activation, which is reflected in standard $G-V$ curves. Thus, we can examine whether the voltage dependence of recombination follows either the $Q-V$ or $G-V$ curves for this mutant ion channel.

Figure 7 shows ionic and gating currents obtained for the conducting and nonconducting variants, respectively, of *Shaker*-IR A359C labeled with BPMTS. The nonconducting mutation W434F has little effect on the gating current (*18*−*20*). We used this mutant rather than removing all permeant ions from the conducting mutant, because permeant ions can have profound consequences for gating (*3*). $G-V$ and $Q-V$ curves were obtained from data similar to those shown, and were fit by Boltzmann functions with parameters given in the legend of Figure 7. These fitted curves are scaled and superimposed on the cross-linking data depicted in Figure 6B. All three functions overlap extensively, although the $G-V$ slope (4.1 e_0) is somewhat greater than observed for both the $Q-V$ curve (2.2 e_0) and the extent of recombination (2.3 e_0). The similarity of the latter two slopes suggests that separation of the alkyl and ketyl free radicals by depolarization is due to S4 movement rather than subsequent movements accompanying the opening of the activation gate. However, the overlapping $G-V$ curve (Figure 6B) makes this conclusion weak. We will attempt to resolve this ambiguity in more detail in the next section of the paper.

We showed above that cross-linking is more efficient at −120 mV than at 30 mV in *Shaker* S4 segments (Figure 2). We also reasoned that the first photochemical step in cross-linking, H-atom abstraction, takes place within a few milliseconds. We do not know the identity of the insertion site of the BP ketone; however, we ask here whether the insertion site is the same or different when H-atom abstraction takes place at a hyperpolarized versus depolarized voltage. If the insertion site is the same, we predict that the inhibition of recombination by a depolarization will be the same, whether the UV flash is given at a hyperpolarized or depolarized voltage. To test this, we performed the following experiment. A flash at either −120 or 10 mV was followed by a 500 ms depolarization to 10 mV. After a 50 ms return to the −120 mV holding potential, the fractional reduction in ionic current was measured, as described in the legend of Figure 6. The fractional current remaining after a flash was 0.652 ± 0.026 ($n = 4$) and 0.680 ± 0.030 ($n = 8$) for UV at 10 and −120 mV, respectively. These values are not significantly different ($P > 0.05$), suggesting that the insertion sites are the same whether the lamp is flashed at a depolarized or a hyperpolarized voltage. Note that the expected remaining current 550 ms after a flash is <0.2 if the voltage is maintained at −120 mV without depolarization (Figure 3B). These results suggest that the different cross-linking rates at the different voltages, observed in Figure 2, are a consequence of different efficiencies of H-atom abstraction from the same insertion site.

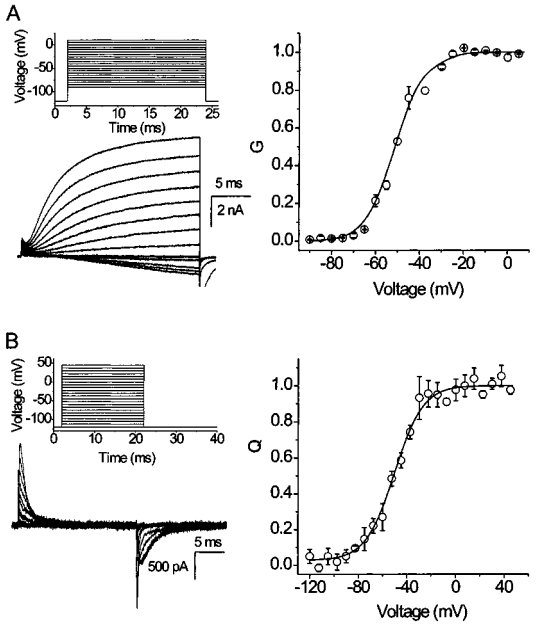

FIGURE 7: Voltage dependence of channel activation in A359C-BP mutant channels and charge movement in W434F/A359C-BP nonconducting channels. (A) Ionic currents and $G-V$ relationship of A359C-BP channels. The left upper panel is the voltage protocol, which has 5 mV increments from −90 to 10 mV with a holding potential of −120 mV. The family of ionic currents is shown in the lower left panel. The right panel is the $G-V$ curve. G was calculated according to the equation $G = I/(V - V_r)$, where I is the ionic current measured at the end of the test pulse and V_r is the reversal potential, which was −38.9 mV in this case. The data were plotted after normalization. The solid line is the fit of a single-Boltzmann function: $G = 1/\{1 + \exp[-q(V - V_{1/2})/kT]\}$. The fit of the $G-V$ curve obtained in five cells resulted in a $V_{1/2}$ of -51.2 ± 1.0 mV and a slope q of 4.1 ± 0.1 e_0. (B) $Q-V$ relationship in nonconducting W434F/A359C-BP channels. The left upper panel is the voltage protocol for gating current measurements, which has 7.5 mV increments from −120 to 45 mV with a holding potential of −120 mV. The left lower panel shows typical on- and off-gating currents plotted from every other test voltage. The right panel shows the $Q-V$ relationship and its fit by a single-Boltzmann function as in panel A. The total gating charge moved (Q) was estimated by numerically integrating the off-gating current at each voltage and was normalized to unity at large depolarizations (see Experimental Procedures). We fitted the $Q-V$ relationship to a single-Boltzmann function, which gave $V_{1/2}$ and q values of -50.4 ± 0.5 mV and 2.2 ± 0.2 e_0, respectively.

Determining the Movement Underlying Free Radical Separation. Although the results depicted in Figure 6B suggest that S4 movement itself, rather than gate movement, separates the free radicals generated by H-atom abstraction,

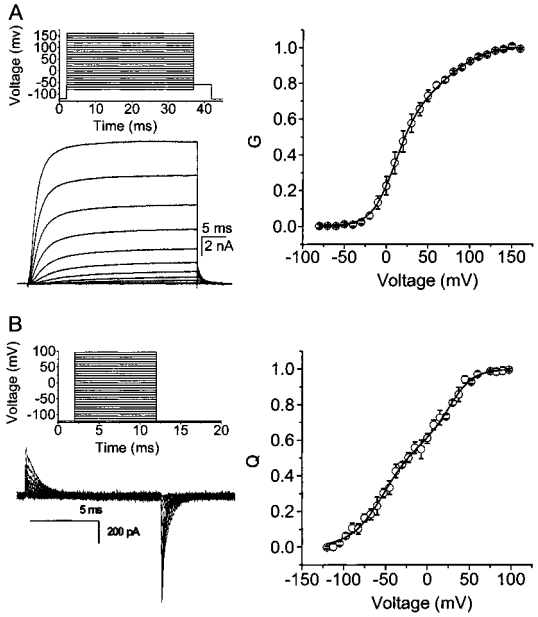

FIGURE 8: Voltage dependence of channel activation in A359C/L382V mutant channels and charge movement in nonconducting A359C/L382V/W434F mutant channels. A359C was labeled with BPMTS. (A) Ionic currents and $G-V$ relationship of A359C/L382V channels. The ionic currents were measured using a high-intracellular K^+ solution due to the low expression levels of the A359C/L382V mutant. We measured the $G-V$ relationship from the tail currents at -60 mV after repolarization from different 35 ms conditioning voltages. The holding potential is -120 mV. The left lower panel shows ionic currents measured with every other conditioning voltage. The right panel shows the $G-V$ relationship. The solid line is a fit of a double-Boltzmann function: $G = A_1/\{1 + \exp[-q_1(V - V_{1,1/2})/kT]\} + A_2/\{1 + \exp[-q_2(V - V_{2,1/2})/kT]\}$. The fitting of a double-Boltzmann function gives $V_{1,1/2}$ and $V_{2,1/2}$ values of -9.6 ± 1.4 and 66.5 ± 11.2 mV, respectively. The values for slopes q_1 and q_2 were 1.93 ± 0.29 and 1.00 ± 0.17 e_0, respectively. The values for A_1 and A_2 were 0.61 and 0.39, respectively. (B) $Q-V$ relationship of BP-labeled A359C/L382V/W434F channels. Gating currents were measured in a high-intracellular Cs^+ solution to avoid contamination by endogenous K^+ currents (see Experimental Procedures), but $Q-V$ relations measured from the two types of intracellular solutions are not distinguishable (*22*). The left upper panel shows the voltage protocol, which has a 10 ms test pulse with various amplitudes from holding potential of -120 to 100 mV with a 7.5 mV increment. The left lower panel shows typical on- and off-gating currents, which were measured from every other test voltage. The right panel shows the $Q-V$ relationship and its fit by a double-Boltzmann function as in panel A, with parameters $V_{1,1/2}$, $V_{2,1/2}$, q_1, q_2, A_1, and A_2 equal to -51.4 ± 4.2 mV, 26.6 ± 3.6 mV, 1.25 ± 0.12 e_0, 1.78 ± 0.35 e_0, 0.61, and 0.39, respectively.

the extensive overlap of the voltage dependence of recombination rate with that of both $Q-V$ and $G-V$ curves leaves the identification of the separating movement ambiguous. To test whether S4 movement or activation gate movement inhibits recombination, we used a *Shaker* mutant (L382V) in which the $Q-V$ and $G-V$ curves are significantly separated along the voltage axis (*21*, *22*). L382 is located at the bottom of the S4 segment, and the L382V mutation shifts the $G-V$ curve strongly ($\sim$50 mV) in a depolarizing direction while broadening the $Q-V$ curve. We combined this mutation with A359C in *Shaker*-IR, using both conducting and nonconducting (W434F) variants to measure $G-V$ and $Q-V$ curves, respectively, as shown in Figure 8. In all cases, A359C was labeled with BPMTS.

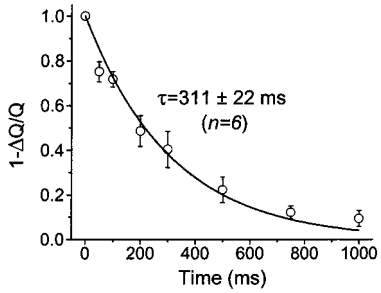

FIGURE 9: Kinetics of S4 segment immobilization of the A359C/V382L mutant. We used the same protocol we used for the A359C mutant (see Figure 3), except with a V_T of 60 mV.

Both $G-V$ and $Q-V$ curves were fit by double-Boltzmann functions. As in previous studies using the L382V mutation, there is minimal overlap between these curves (see below). Activation gates only open significantly at positive membrane potentials, whereas more than 50% of the gating charge moves at negative voltages (Figure 8). These results suggest that channel opening requires substantial S4 movement at negative voltages, consistent with previous studies (*21*, *22*). This separation of charge movement and activation gating allows us to test whether the inhibition of recombination tracks S4 movement or channel opening.

We first examined whether slow cross-linking kinetics are also observed in the A359C/L382V double mutant. Using an experimental protocol similar to that shown in Figure 3A, except for a V_T of 60 mV, we measured recombination kinetics at -120 mV (Figure 9). The time constant of photo-cross-linking is $\sim$310 ms, 1.2-fold larger than that of the A359C mutant, confirming that cross-linking is slow, and suggesting that the L382V mutation affects the local environment of BP-labeled A359C at the extracellular end of the S4 segment.

We then measured the voltage dependence of recombination (Figure 10). As in the A359C single mutant, recombination in the double mutant was monotonically inhibited by depolarization, and in the double mutant the data clearly tend to follow the $Q-V$, rather than the $G-V$, relationship. We fit the $(1 - \Delta Q/Q) - V$ relationship to a double-Boltzmann function plus a constant with the same values of $V_{1,1/2}$ and $V_{2,1/2}$ as in the $Q-V$ curve. The adjustable parameters were the amplitudes and slopes of each component. The near superposition of these two functions further supports the idea that S4 movement itself is responsible for inhibiting recombination, rather than a subsequent movement associated with opening of the activation gate. Moreover, the agreement between charge movement and inhibition of recombination is particularly evident at negative voltages, where the so-called Q_1 component dominates (*23*). This suggests that the critical movement separating the ketyl−alkyl radical pair occurs in the early transitions of the activation pathway. These results add further support to the idea that S4 movement underlies the bulk of charge movement.

DISCUSSION

Benzophenone (BP) photoprobes, because of their distinct chemical and biochemical advantages, have been widely used in protein, nucleic acid, and lipid biochemistry (*9*, *24*). Upon excitation by UV light, the ketone group of the BP moiety

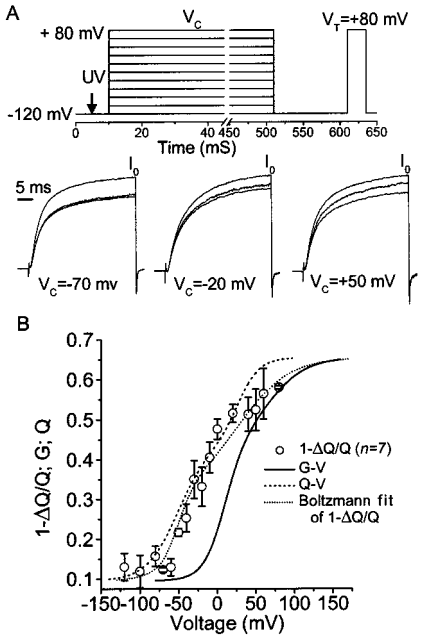

FIGURE 10: Voltage dependence of S4 segment immobilization of the BP-labeled A359C/L382V mutant. (A) The voltage protocol (upper panel) and typical currents (lower panel) with different V_C values showing different reductions after irradiation. (B) The $(1 - \Delta Q/Q) - V$ relation (○) ($n = 7$). The solid curve represents a fit of a double-Boltzmann function plus a constant: $1 - \Delta Q/Q = A_0 + A_1/\{1 + \exp[-q_1(V - V_{1,1/2})/kT]\} + A_2/\{1 + \exp[-q_2(V - V_{2,1/2})/kT]\}$. The estimated values of A_0, A_1, A_2, q_1, and q_2 are 0.095, 0.22, 0.34, 2.31 e_0, and 0.77 e_0, respectively. $V_{1,1/2}$ and $V_{2,1/2}$ were fixed to the values from the $Q-V$ curve of A359C/L382V/W434F mutant channels (see Figure 8). The dotted and dashed lines are normalized $G-V$ and $Q-V$ curves from Figure 8, respectively.

is capable of inserting into C−H bonds, covalently linking the BP with a neighboring structure. We recently designed and characterized the bifunctional cysteine reagent BPMTS in an ion channel study that employed molecular biology, electrophysiology, and UV irradiation (*8*). This approach allowed us to selectively immobilize different moving parts, either voltage sensors or gates, of the channel.

One of our goals in these studies is to trap the channel in particular gating states. In voltage-gated ion channels, the conformational states caused by changes in membrane potential may have very brief lifetimes, on a time scale similar to the lifetime of the triplet state $T_1(n,\pi^*)$ of BP (<1 ms). For this reason, we measured the kinetics of cross-linking in this study, and we were surprised to find that immobilization was at least 2 orders of magnitude slower than the triplet state lifetime. It is important to emphasize here that we are not measuring the level of cross-linking directly. We are measuring the effects of UV irradiation on the biophysical properties of voltage-gated ion channel currents. In this study, the effects are always a decrease in the magnitude of ionic currents. The assumption that these decreases are due to the cross-linking itself, rather than subsequent, slower allosteric consequences of cross-linking, is based on the results of our previous study (*8*), where we described the detailed effects of immobilizing both voltage sensors and gates. For example, the inactivation gate of the Na^+ channel can be selectively immobilized either open or closed, and there is a fourth-power relationship between the reduction of gating and ionic current when irradiating the *Shaker* mutant A359C, as predicted by the tetrameric

Table 1:

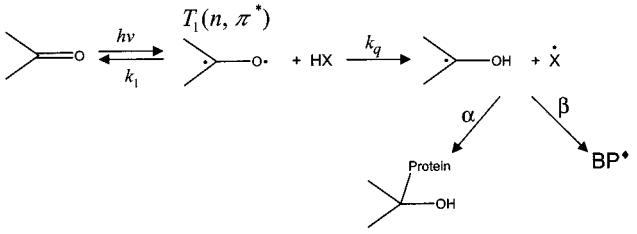

a	*Shaker* A359C flashed at −120 mV	*Shaker* A359C flashed at 30 mV	$Na_v1.4$ D2:R1C flashed at −140 mV
k_q (s^{-1})	1740	650	1670
α (s^{-1})	1.11	1.18	41.9
β (s^{-1})	2.71	2.63	18.0
$\tau_{T_1,S4}$ (μs)	85.2	93.9	85.7

[a] Photochemical rate constants. The rate constants k_q, α, and β of the reaction scheme shown above were estimated from the rates and efficiencies of cross-linking, as described in the text. We set k_1 equal to 10^4 s^{-1} (*9*). H-Atom abstraction is assumed to lead irreversibly either to successful immobilization with a rate α or to a failure to immobilize with a rate β. The failure could be due, for example, to oxidation of one of the free radicals before recombination or to insertion into a site that does not immobilize the S4 segment. The lifetime in the excited state $\tau_{T_1,S4} = (k_1 + k_q)^{-1}$.

symmetry of the channels. These effects are not only consistent with the expectations for immobilizing the moving part under study but also completely unique, in that similar biophysical consequences are not observed either for mutations of the residues in question or for covalent modification of the introduced cysteines by any reagent, whether charged, neutral, small, or as large as tetramethylrhodamine maleimide (*25*). Therefore, although we do not have a direct measurement of the insertion of the activated ketone, a parsimonious interpretation of our data is that current reduction is an immediate consequence of cross-linking the S4 segment to a neighboring region of the channel, thus immobilizing it. As we showed previously, this immobilization is complete with respect to the charge movement expected to be carried by an individual S4 segment (*8*).

Our data strongly suggest that the rate-limiting step in cross-linking is the recombination of the ketyl−alkyl radical pair produced by H-atom abstraction from the triplet excited state $T_1(n,\pi^*)$. The lifetime of $T_1(n,\pi^*)$ in the absence of an H-atom donor (k_1^{-1}; see the photochemical scheme in Table 1) is in the range of 100−700 μs at room temperature (*9*, *10*). However, the lifetime may be reduced substantially in the presence of an H-atom donor. We can roughly estimate the lifetime of $T_1(n,\pi^*)$ for our S4 experiments from the cross-linking efficiency for a single flash, as follows.

We assume that the principle quenching reaction of the triplet excited state is H-atom abstraction. This must be the case when cross-linking efficiency is >70%, as we have observed for particular cysteine mutants (*8*), and has been observed for other BP derivatives (*9*). The rate constant k_q for H-abstraction depends on the local environment of the tethered BP moiety (*10*). The resultant ketyl−alkyl radical pair has two irreversible fates that interest us here (Table 1). Either recombination successfully immobilizes the S4 segment at a rate α, or it does not with a rate β (*8*). Failure of immobilization is a consequence of any of a number of

irreversible chemical reactions. For example, the target of H-atom abstraction may be a region of the protein or, for example, lipid that cannot result in immobilization, even if recombination is successful. Another possibility for failure is that either the alkyl or ketyl free radical might react with another substrate before recombination occurs.

The fraction of S4 segments immobilized by a single flash of light (F_{immob}) is given directly by the fractional current reduction ($F_{decrease}$) in the case of the Na^+ channel mutant D2:R1C or, because of tetrameric symmetry in *Shaker*, by

$$F_{immob} = 1 - (1 - F_{decrease})^{1/4}$$

We estimate $w = \alpha/(\alpha + \beta)$ from the steady state S4 immobilization after saturating exposure to UV light (e.g., Figure 2B, and Figure 2D in ref *8*). The total fraction F_H of BPs that undergo H-atom abstraction after a single flash is F_{immob}/w. Finally, we can estimate k_q as follows.

$$k_q = \frac{F_H}{1 - F_H} k_1$$

The lifetime in the triplet excited state is given by $(k_1 + k_q)^{-1}$. We also estimate the rate constants α and β from the recombination time constants [$\tau = (\alpha + \beta)^{-1}$] of Figures 3 and 4. All of these estimates are presented in Table 1 for *Shaker*-IR A359C, irradiated at two different voltages, and for the Na^+ channel.

The estimates in Table 1 lead to a number of conclusions. First, the rate of H-atom abstraction is 2.7-fold larger at a hyperpolarized than at a depolarized voltage in *Shaker*. This explains the slower time constant for current reduction when irradiating at the depolarized voltage (Figure 2). This is probably because of a change in the position or orientation of the BP adduct by the S4 segment when the voltage is changed. Second, the rate of H-atom abstraction at a hyperpolarized voltage is similar for *Shaker* and Na^+ channels, although the recombination rate α is >30-fold larger for the Na^+ channel S4 segment. This difference in α is likely to be due to the structural differences near the external ends of these two S4 segments. Third, recombination is more efficient for Na^+ channels, where $\alpha > \beta$. In *Shaker*, $\beta > \alpha$. Part of the increased insertion efficiency for Na^+ channels is due to the higher estimate for α in this channel than in *Shaker*. Finally, quenching by H-atom donors has only a small effect on the excited state lifetime, reducing it by at most 15% in the absence of quenching.

Although recombination or immobilization is much slower than the lifetimes of many of the gating states of Na^+ and K^+ channels, the rapidity of H-atom abstraction allows us to initiate the irreversible pathway to immobilization with a similar rapidity. Once H-atom abstraction has taken place, BP's insertion target is chosen, because each BP group is tethered and unable to reach free radicals generated by other tethered BP moieties.[2] Therefore, state-dependent cross-linking is feasible, even for very short-lived gating states, because it is possible to time the initial photochemical reaction to the occurrence of a particular gating state of the channel, even if the recombination occurs much later. In this study, we used the divergent kinetics of abstraction and recombination to test whether voltage-dependent movement was able to separate the ketyl−alkyl radical pair, thus inhibiting recombination. The ability to do so (Figures 6 and 10) provided us the opportunity to ask about voltage-dependent movements in the vicinity of the BP tethered to a *Shaker* S4 segment.

The agreement between the voltage dependence of charge movement and that of inhibition of recombination is rather striking, both in the A359C mutant and in the A359C/L382V double mutant, which has strongly altered charge movement and activation gating. This further supports the idea that the movement separating the two free radicals is the same movement that translocates gating charge. Therefore, it is the S4 movement through the electric field that appears to inhibit recombination, not a downstream consequence of this charge movement, such as a movement of the insertion site due to opening of the activation gate. This result is in accord with fluorescence measurements of the *Shaker* A359C mutant labeled with tetramethylrhodamine maleimide (*25*, *27*). Voltage-dependent changes in fluorescence emission, which are due primarily to voltage-dependent quenching in the local vicinity of the fluorophore (*27*), follow the $Q-V$ curve rather faithfully (*25*, *27*).

Why Is Recombination So Slow? Organic free radicals are highly reactive species, especially with one another. In solution, the recombination of carbon free radicals is typically diffusion-limited; therefore, free radicals are often very short-lived (*28*, *29*). Recombination on the time scale of a few microseconds has been reported for the ketyl−alkyl radical pair produced by BP (*30*). These facts lead to two questions. Why do we observe recombination on a time scale of tens to hundreds of milliseconds, and why are the free radicals so stable?

Recombination has two requirements. First, the two just-formed radicals that were generated from an excited triplet state of BP are in an unpaired triplet state and must undergo a spin inversion before they can recombine in a singlet configuration. This triplet−singlet interconversion typically takes <1 μs (*31*) and, therefore, is unlikely to contribute to the slow cross-linking kinetics we observe. Second, a favorable geometry is needed for efficient recombination of the ketyl and alkyl radicals, as it is for H-atom abstraction. However, the optimal geometric configurations between the BP ketone and its C−H target are not the same for these two sequential photochemical reactions. If there is any steric hindrance in obtaining the optimal configuration for recombination, its rate may decrease dramatically. In this case, the free radicals, sometimes called "persistent radicals", may exist for minutes or longer (*29*). Steric hindrance is likely to be the reason for the slow recombination rates we measured, especially for *Shaker* S4 segments. Neither the alkyl nor the ketyl free radical is free to diffuse to interact with one another, or with other substrates. Furthermore, it is reasonable to imagine local constraints on the mobility of both the tethered BP and its target. Evidently, these constraints are greater for recombination in *Shaker* than in Na^+ channel S4 segments, leading to the ~16-fold larger rate in Na^+ channels. Interestingly, the efficiency of cross-linking is also ~6-fold greater for Na^+ channels. This could be due in part to the fact that other radical-destroying

[2] The closest distance between S4 segments of *Shaker* is ~28 Å (*26*), compared with the ~10 Å linker between BP and its attached cysteine.

reactions have more time to take place in *Shaker* because of its slow recombination rate. In general, the rates of reactions between radicals and nonradical substrates are much slower than those between two radicals (*29*).

CONCLUSION

The rapid H-atom abstraction and slow recombination of BP-induced cross-linking of S4 segments provide us the opportunity to kill two birds with one stone. On one hand, we can trap short-lived gating states with careful timing of brief UV flashes. On the other hand, we can explore the nature of the movements near the S4 segment by comparing the voltage dependence of inhibition of recombination with that of charge movement and gating.

We envisage two extensions of this approach. First, it may be possible to immobilize S4 segments by introducing cysteines at other sites on S4 segments. If so, we can explore the nature of voltage-dependent conformational changes both along and around the S4 segment. This approach is complementary to either cysteine accessibility scanning (*32*), histidine scanning (*33*), or fluorescence scanning (*34*). Second, this method may be used with channel gates, which can also be immobilized in a state-dependent manner (*8*). Together, these techniques will provide insight into the molecular rearrangements of ion channels as they respond to the stimuli that open and close their gates.

ACKNOWLEDGMENT

We thank Dr. Manuel Covarrubias for insightful comments on the manuscript.

REFERENCES

1. Hille, B. (1992) *Ionic Channels of Excitable Membranes*, Sinauer Associates Inc., Sunderland, MA.
2. Sigworth, F. J. (1994) *Q. Rev. Biophys. 27*, 1−40.
3. Yellen, G. (1998) *Q. Rev. Biophys. 31*, 239−295.
4. Bezanilla, F. (2000) *Physiol. Rev. 80*, 555−592.
5. Horn, R. (2000) *Biochemistry 39*, 15653−15658.
6. Catterall, W. A. (1986) *Annu. Rev. Biochem. 55*, 953−985.
7. Catterall, W. A. (2000) *Neuron 26*, 13−25.
8. Horn, R., Ding, S., and Gruber, H. J. (2000) *J. Gen. Physiol. 116*, 461−475.
9. Dormán, G., and Prestwich, G. D. (1994) *Biochemistry 33*, 5661−5673.
10. Turro, N. J. (1991) *Modern Molecular Photochemistry*, University Science Books, Sausalito, CA.
11. Melishchuk, A., Loboda, A., and Armstrong, C. M. (1998) *Biophys. J. 75*, 1828−1835.
12. Yang, N., and Horn, R. (1995) *Neuron 15*, 213−218.
13. Larsson, H. P., Baker, O. S., Dhillon, D. S., and Isacoff, E. Y. (1996) *Neuron 16*, 387−397.
14. Yang, N., George, A. L., Jr., and Horn, R. (1996) *Neuron 16*, 113−122.
15. Seoh, S. A., Sigg, D., Papazian, D. M., and Bezanilla, F. (1996) *Neuron 16*, 1159−1167.
16. Sigg, D., and Bezanilla, F. (1997) *J. Gen. Physiol. 109*, 27−39.
17. Lopez-Barneo, J., Hoshi, T., Heinemann, S. H., and Aldrich, R. W. (1993) *Recept. Channels 1*, 61−71.
18. Perozo, E., MacKinnon, R., Bezanilla, F., and Stefani, E. (1993) *Neuron 11*, 353−358.
19. Yang, Y. S., Yan, Y. Y., and Sigworth, F. J. (1997) *J. Gen. Physiol. 109*, 779−789.
20. Roux, M. J., Olcese, R., Toro, L., Bezanilla, F., and Stefani, E. (1998) *J. Gen. Physiol. 111*, 625−638.
21. Schoppa, N. E., McCormack, K., Tanouye, M. A., and Sigworth, F. J. (1992) *Science 255*, 1712−1715.
22. Schoppa, N. E., and Sigworth, F. J. (1998) *J. Gen. Physiol. 111*, 295−311.
23. Bezanilla, F., Perozo, E., and Stefani, E. (1994) *Biophys. J. 66*, 1011−1021.
24. Dormán, G., and Prestwich, G. D. (2000) *Trends Biotechnol. 18*, 64−67.
25. Mannuzzu, L. M., Moronne, M. M., and Isacoff, E. Y. (1996) *Science 271*, 213−216.
26. Cha, A., Snyder, G. E., Selvin, P. R., and Bezanilla, F. (1999) *Nature 402*, 809−813.
27. Cha, A., and Bezanilla, F. (1997) *Neuron 19*, 1127−1140.
28. Alfassi, Z. B. (1988) in *Chemical Kinetics of Small Organic Radicals* (Alfassi, Z. B., Ed.) pp 129−144, CRC Press, Boca Raton, FL.
29. Walling, C. (1996) in *Energetics of Organic Free Radicals* (Simoes, J. A., Greenberg, A., and Liebman, J. F., Eds.) pp 1−21, Chapman & Hall, London.
30. Eveson, R. W., Timmel, C. R., Brocklehurst, B., Hore, P. J., and McLauchlan, K. A. (2000) *Int. J. Radiat. Biol. 76*, 1509−1522.
31. Steiner, U. E., and Ulrich, T. (1989) *Chem. Rev. 89*, 51−147.
32. Karlin, A., and Akabas, M. H. (1998) *Methods Enzymol. 293*, 123−145.
33. Starace, D. M., Stefani, E., and Bezanilla, F. (1997) *Neuron 19*, 1319−1327.
34. Gandhi, C. S., Loots, E., and Isacoff, E. Y. (2000) *Neuron 27*, 585−595.

BI010709Y